22nd International Conference on Renewable Energies and Power Quality (ICREPQ'24)
Bilbao (Spain), 26th to 28th June 2024

ISBN: 978-84-09-60656-6

Tuning of Speed PI in FCSMPC of Multi-phase Drives using Pareto

F. Barrero[1], M.G. Satué[2] and M. Perales[1]

[1] Department of Electronic Engineering
[2] Department of System and Automation Engineering
E.T.S.I., University of Sevilla
Camino de los Descubrimientos sn, 41092 Sevilla (Spain)
Phone/Fax number: +0034 954 487372

Abstract. Control of drives is often done using an outer speed loop and an inner current loop. The outer loop is mostly performed by a PI controller. Its tuning is not trivial. In this paper a Pareto analysis is proposed to reveal trade-offs between figures of merit. The drive used for the study includes a 5-phase induction motor supplied by a voltage source inverter. A finite-state predictive method is used for the inner loop (current control). The analysis is done experimentally, thus including all sorts of non-idealities not appearing in commonly found models. The importance of the result lies in showing that arbitrary performance enhancements are not possible in a general case.

Keywords. Application of power electronics, Digital implementation, Modeling and simulation of power systems, PI control, Tuning.

1. Introduction

PI controllers are routinely used in variable speed drives for speed and/or current regulation. The speed control loop (outer loop) is used to maintain the mechanical speed close to its reference value. The current loop has a much faster time scale and is used to produce stator currents that, in turn, produce a torque that drives the speed. In the last few years, there has been a trend in academia to replace PI loops with more sophisticated alternatives such as Model Predictive Control (MPC). This trend is a consequence of the relative success attained by MPC in other realms [1], [2]. The case of predictive control of drives is exemplified by the so-called Finite State Model Predictive Control (FSMPC), where direct digital control of the Voltage Source Inverter (VSI) is attained. In FSMPC the Pulse Width Modulation (PWM) stage is no longer necessary, thus improving the performance of the system as reported in [3] and [4].

Going back to the speed control loop, the influential works related to PI tuning for Indirect Field Oriented Control (IFOC) date from the 1990s and 2000s [5]-[7]. These works provide methods that utilize some, not very strict, requirements on knowledge of the time constant of the rotor of the IM to guarantee global stability. A dynamic model of the current-fed IM is used as the basis of these methods. Some variations have been reported using harmonic injection [8], but, in most cases, the models do not consider practicalities such as nonlinearities in the dynamics of IM, the behavior of VSI+modulation, and aspects derived from the use of a Digital Signal Processor (DSP) for PI+IFOC algorithms.

In the 20 years that followed, the state of the art has been enriched by some papers that expanded the previous works in a variety of ways. Most of the efforts have focused on: sensorless operation, estimation of the rotor time constant, extension of the PI with operating-point based scheduling and/or adaptivity, fault-tolerant capabilities, and tuning methods based on extensive simulation/experimentation. Other technologies have even been proposed to replace the speed PI but, despite all of this, conventional PI control is still reported as competitive due to its simple implementation compared with nonlinear control [9], adaptive control [10], robust control [11]-[12] and some fuzzy and/or neural approaches [13]-[15]. The lack of theoretical models to analyze the above cited practical aspects and their influence on complex figures of merit such as the Integral Time-multiplied Absolute Error (ITAE) has led to the use of an experimental approach for the PI tuning. For example, metaheuristic optimization algorithms are used in [16] to optimize the PI.

Moreover, in recent years, there has been a technological advance in the drives themselves. Motors have moved from 3-phase to multiphase machines and from two-level to multilevel VSIs [17]. The multiphase case is especially interesting for this study, as the overall structure of the controller is IFOC-like. The interaction among phases makes the tuning of the inner loop PI more complex. Multiphase drives require at least four PI controllers for the PWM method and only one predictive controller for FSMPC. In particular, the existence (in stator currents of multiphase IM) of a torque producing plane ($\alpha-\beta$) and various harmonic planes (x_j-y_j with $j\geq1$) makes the control design more challenging. For instance, modulation schemes for 5 and 6-phase drives have little to do with each other, yet predictive controllers have the same structure for both. Therefore, FSMPC has made the problem more tractable, but at the cost of increased computational needs [18]-[19]. In addition, the FSMPC method is becoming popular due to its flexibility. For instance, modulation variants that are impossible with PWM can be used with FSMPC [20]-[21], the mechanical load characteristics can be considered with ease, and the fault tolerance capabilities are better utilized [22]. State estimation methods such as Kalman filtering and observers can also be incorporated with ease in MPC approaches [23]-[24], expanding its potential with respect to the PI case.

Speed PI tuning can, in theory, make use of an accurate model of the IM. However, some aspects have been resistant to modeling. This is the case of the delay introduced by the modulation technique used (PWM or its variants, or even FSMPC). Saturation in some variables (currents, fluxes, etc.) has also not been considered in many cases, and mechanical speed sensing can also introduce delay [25]-[26]. Finally, some figures of merit, such as torque ripple, are typically not considered in the automatic control community, yet they play a crucial role in applications. In this context there is not a set of equations (or other convenient procedure) to link figures of merit with controller parameters. The proposal of this paper considers a reduced set of indices to assess controllers for the inner loop of drives. These indices summarize the behavior of the system, as other indices are related to the set. Then, all possible controller tunings are considered. The Pareto-optimal solutions are then shown to pertain to a surface of lower dimension. As a result, any PI tuning must either be dominated (not Pareto-optimal) or lie in the surface.

2. IFOC Structure used in the Experiments

In the indirect field-oriented control scheme, flux and torque are independently regulated. The flux current set point i_d^* is set to magnetize the motor whereas quadrature current i_q^* is used to manipulate the produced torque. The PI in the velocity feedback loop is responsible for generating i_q^* to drive the mechanical speed control error to zero.

$$i_q^* = k_p \cdot e + k_i \cdot \int_0^\infty e(\tau) d\tau \qquad (1)$$

where $e = \omega^* - \omega_m$ is the velocity error or difference between the speed set point (ω^*) and the speed measurement (ω_m).

Once the set points in the d–q coordinates are known, they are projected to the α–β space using the Park transformation, obtaining a reference for the stator current in α–β plane as $I_{\alpha-\beta}^* = \mathrm{D}\left(i_d^*, i_q^*\right)^T$, where matrix D is given by

$$\mathrm{D} = \begin{pmatrix} cos\theta_e & sin\theta_e \\ -sin\theta_e & cos\theta_e \end{pmatrix} \qquad (2)$$

The flux position θ_e is estimated as $\theta_e = \int \omega_e \, dt$, where $\omega_e = \omega_{sl} + P \cdot \omega_m$, being P the number of pairs of poles of the IM and the slip frequency:

$$\omega_{sl} = \frac{i_q^*}{i_d^*} \cdot \frac{1}{\hat{\tau}_r} \qquad (3)$$

where $\hat{\tau}_r$ is an estimation of the rotor time constant $\frac{L_r}{R_r}$, being L_r and R_r the inductance and the resistance of the rotor, respectively. As a result, the set point for stator current tracking $i^*(k)$ has an amplitude $I^* = \sqrt{{i_d^*}^2 + {i_q^*}^2}$. Finally, the α–β references can be expressed as $i_\alpha^*(t) = I^* sin\omega_e t$, $i_\beta^*(t) = I^* cos\omega_e t$, $i_x^*(t) = 0$, $i_y^*(t) = 0$ (note that a distributed winding machine is considered).

A. FSMPC Control of a 5-phase IM

The inner loop of an IFOC scheme is responsible for producing stator currents in α–β that follow their references and, at the same time, maintaining x–y currents close to zero, as they do not produce torque but contribute to losses. This task can be accomplished using the FSMPC strategy. A model of the IM is needed to predict the IM behavior for each possible VSI configuration. Using the vector space decomposition, the 5-phase stator currents are projected in the energy conversion plane (α–β) and the harmonic plane (x–y), resulting in equations relating stator voltages, $v_s(t)$, stator and rotor currents, $i_s(t)$ and $i_r(t)$, fluxes, $\psi_s(t)$ and $\psi_r(t)$, and rotor electrical angular speed $\omega_r(t) = P \cdot \omega_m(t)$ as follows:

$$\begin{aligned} v_{\alpha\beta s}(t) &= R_s\, i_{\alpha\beta s}(t) + p\psi_{\alpha\beta s}(t) \\ 0 &= R_r\, i_{\alpha\beta r}(t) + p\psi_{\alpha\beta r}(t) - j\omega_r(t)\psi_{\alpha\beta r}(t) \\ \psi_{\alpha\beta s}(t) &= L_s\, i_{\alpha\beta s}(t) + L_m\, i_{\alpha\beta r}(t) \\ \psi_{\alpha\beta r}(t) &= L_m\, i_{\alpha\beta s}(t) + L_r\, i_{\alpha\beta r}(t) \\ v_{xyzs}(t) &= R_s\, i_{xyzs}(t) + p\psi_{xyzs}(t) \\ \psi_{xyzs}(t) &= L_{ls}\, i_{xyzs}(t) \end{aligned} \qquad (4)$$

where p is the derivative operator, and the following machine parameters are used: resistances R_s, R_r, inductances L_s, L_r, leakage inductance L_{ls} and mutual inductance L_m. Sub-index s stands for stator and r for rotor. Stator voltages are produced by VSI according to the gating signals K_j for the VSI legs j=1, ..., 5 accommodated in u=(K_1, ..., K_5) ∈ B^5 with B={0,1}. The resulting voltages $v_{\alpha\beta xyzs}$ are

$$v_{\alpha\beta xyzs} = \left(v_{\alpha s}, v_{\beta s}, v_{xs}, v_{ys}, v_{zs}\right) = \frac{2}{25} V_{DC} \mathbf{TM} u \qquad (5)$$

where V_{DC} is the DC link voltage, **T** is a connectivity matrix that keeps invariant the original values of the electrical variables after the transformation but not the total powers, and **M** is a coordinate transformation matrix accounting for the spatial distribution of machine windings.

$$\mathbf{TM} = \begin{pmatrix} d & \gamma_1^c & \gamma_2^c & \gamma_3^c & \gamma_4^c \\ 0 & \gamma_1^s & \gamma_2^s & \gamma_3^s & \gamma_4^s \\ d & \gamma_2^c & \gamma_4^c & \gamma_6^c & \gamma_8^c \\ 0 & \gamma_2^s & \gamma_4^s & \gamma_6^s & \gamma_8^s \\ c & c & c & c & c \end{pmatrix} \begin{pmatrix} a & b & b & b & b \\ b & a & b & b & b \\ b & b & a & b & b \\ b & b & b & a & b \\ b & b & b & b & a \end{pmatrix} \qquad (6)$$

The coefficients used are: $a = 4, b = -1, c = 1/2, d = 1$, $\gamma_h^c = cosh\vartheta, \gamma_h^s = sinh\vartheta, \vartheta = 2\pi/5$ for the five phase IM. The actual values of the electrical parameters corresponding to the machine used in the experiments are given in Table I.

Table I. - Parameters of the five-phase IM

Parameter	Value	Unit
Stator resistance, R_s	12.85	Ω
Rotor resistance, R_r	4.80	Ω
Stator leakage inductance, L_{ls}	79.93	mH
Rotor leakage inductance, L_{lr}	79.93	mH
Mutual inductance, L_m	681.7	mH
Rotational inertia, J_m	0.02	kg m^2
Number of pairs of poles, P	3	-

In discrete time k, the control action $u(k+1)$ is computed minimizing a cost function J. The cost function penalizes the stator currents tracking error as $J = \|i^*(k+2) - \hat{\imath}(k+2)\|^2$, where $\hat{\imath}(k+2)$ are the predicted currents. Note the one sampling period delay due to computations.

The developed electrical torque is derived from the actual values of the direct and quadrature stator currents as

$$T_e = \frac{5}{2} P \frac{L_m^2}{L_{lr}+L_m} \cdot i_d i_q \qquad (7)$$

3. Experiments

The PI tuning is assessed in this section by means of tests in the experimental setup described below.

A. Laboratory Setup

The laboratory arrangement depicted in Fig. 2 is used. A five-phase motor with parameters shown in Table I is powered by a five-phase VSI constructed from two three-phase SEMIKRON SKS 22F modules. A 300V DC power supply is used in the DC-link. The control programs run on a MSK28335 board housing a TMS320F28335 DSP. Hall effect sensors (LH25-NP) are used to measure the stator phase currents. Last, a DC motor is used sharing the same shaft as the IM to provide an opposing torque load (T_L) for the tests.

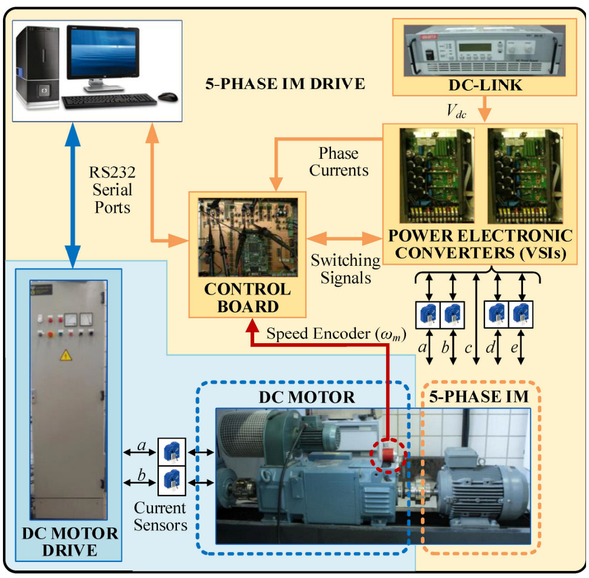

Fig. 1. Diagram and photographs of the laboratory setup used in the experiments.

B. Performance indices

The assessment of variable speed drives can be based on a variety of quantitative criteria. Different applications might put more emphasis on some indices than others. In this paper, three indices are selected, being other indices related to this reduced set. The proposed indices can be obtained experimentally from a step test. The first one is the percentage overshoot PO, defined for an underdamped system as

$$\mathrm{PO} = 100 \frac{\max(\omega - \omega^*)}{\omega^*} \qquad (8)$$

The second index is the rise time (from 0% to 100%) defined as the time required to cross the ω^* value for the first time.

$$\mathrm{RT} = \underset{t \geq 0}{\operatorname{argmin}}(\omega^*(t) - \omega(t)) \qquad (9)$$

The final index is the torque ripple, that is defined as

$$\mathrm{Q_T} = \sqrt{\frac{1}{N}\sum_{k=1}^{N}(T^*(k) - T(k))^2} \qquad (10)$$

The set of all three indices will be represented as a vector:

$$\Gamma = (\mathrm{PO}, \mathrm{RT}, \mathrm{Q_T}) \qquad (11)$$

C. Pareto Surface

A set of step tests are performed on the 5-phase IM to obtain the figures of merit for various combinations of the PI parameters (k_p, k_i). The obtained triples Γ for each PI tuning are recorded. Then, a process of elimination is used to exclude the triples that are not Pareto-optimal. The surviving ones are presented in Fig. 2, where a 3D plot (upper right corner) shows the Γ values and three 2D projections show: γ_2 vs. γ_1 (upper left), γ_3 vs. γ_1 (lower left) and γ_3 vs. γ_2 (lower right). The points are presented in color for better visualization. The color has been linked to γ_3 to provide a sense of elevation. A red color indicates a high value of γ_3 and a blue color indicates a low value of γ_3.

It is interesting to see that the Γ triples are situated approximately on a cubic Titeica surface [27]. The surface is determined mathematically by

$$\gamma_1 \cdot \gamma_2 \cdot \gamma_3 = \bar{\Pi} \qquad (12)$$

where $\bar{\Pi}$ =0.0148 for this case. The repercussions of these findings are deep: by PI tuning alone it is impossible to enhance all figures of merit simultaneously past the Pareto front. Since $\gamma_1 \cdot \gamma_2 \cdot \gamma_3$ is (approximately) a constant, reducing γ_1 will result in an increase in $\gamma_2 \cdot \gamma_3$. The same argument holds for a reduction in either γ_2 or γ_3. Going back to the tuning problem, it is interesting to notice that a particular point in the Pareto front minimizes the distance to the origin. This particular solution (Γ^0) achieves:

$$\|\Gamma^0\|^2 = \min\,({\gamma_1}^2 + {\gamma_2}^2 + {\gamma_3}^2) \qquad (13)$$

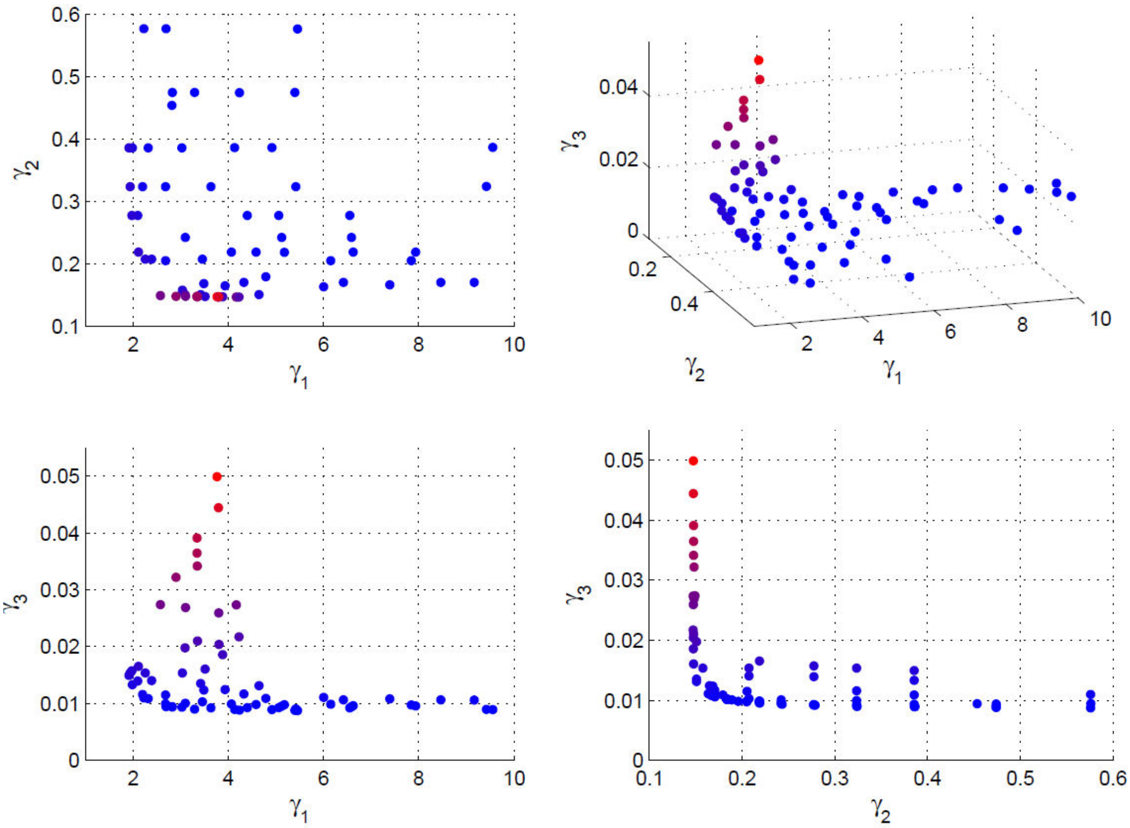

Fig. 2. Pareto front (upper right corner) and 2D projections for ω^{*}=500 (rpm). Color is used to indicate γ_3 values for better visualization.

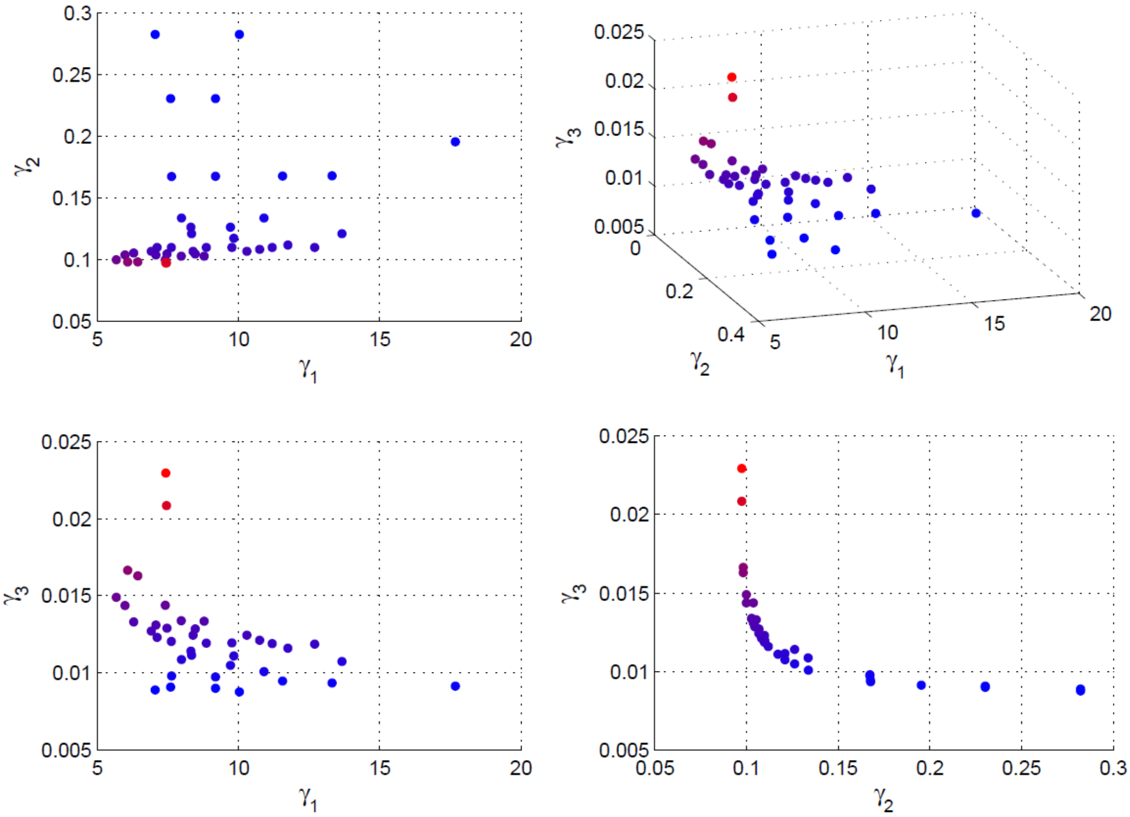

Fig. 3. Pareto front (upper right corner) and 2D projections for ω^{*}=250 (rpm). Color is used to indicate γ_3 values for better visualization.

This solution is optimal if the control objectives (figures of merit) are equally important. This might not be the case in a practical application. Instead, a weighted metric should be used. This is easily achieved by applying scale factors to each figure of merit. For the sake of clarity, the distance of eq. (13) will be used. In this case, the solution closest to the origin (denoted as Γ^0) is found to be Γ^0=(3.3, 0.17, 0.0120). If one chooses to tune the PI to achieve Γ^0, the tuning problem has a definite answer. This is a step forward from various previous works in which the existence of limits for tuning is not realized.

D. Influence of the operating regime

So far, only an operating point has been analyzed. The method is now extended to other values of ω^* to check to what extent the Pareto surface and optimal tuning are affected.

Figure 3 presents the Pareto front and its projections for ω^*=250 (rpm). It can be seen that the Pareto-optimal solutions still lie (approximately) on a Titeica surface. However, for this operating point, the figures of merit have different values. This can be seen by comparing Fig. 2 with Fig. 3, and also in Table II. In the said table, various speed references are considered. For each one, the PI tuning that yields Γ^0 is provided along the actual values of γ_i^0 and the $\overline{\Pi}$ parameter. It can be seen that the optimal tuning is different for each operating point. This supports the adoption of scheduling solutions such as in [28].

In most cases, however, a single PI tuning is used. The particular tuning can be found by trial and error aiming at improving performance near the nominal operating point. This, of course, has the effect of diminished performance far from said nominal point. This is illustrated in Table III, where two PI tunings are compared in terms of the figures of merit for each speed regime. The tuning T1 corresponds to the optimal tuning for 500 rpm ($k_p = 65 \cdot 10^3$, $k_i = 100 \cdot 10^5$), whereas T2 uses as PI parameters the mean value over the various speed regimes, producing ($k_p = 89 \cdot 10^3$, $k_i = 86 \cdot 10^5$). It can be appreciated that the results are not so different, and the degradation with respect to the optimal case might be acceptable in many applications. This provides support for the usual engineering practice used for tuning. However, for high-end applications, the results of this paper show that PI tuning has limits and that something else is needed to provide high performance at all operating points. This is a powerful result that cannot be deduced without the Pareto analysis.

Table II. - Optimal tunings for different operating points

ω^*	$k_p^0 \cdot 10^3$	$k_i^0 \cdot 10^5$	γ_1^0	γ_2^0	γ_3^0	$\overline{\Pi}$
500	65	100	3.3	0.17	0.0120	0.0148
375	42	107	5.3	0.17	0.0103	0.0114
250	120	80	7.1	0.11	0.0123	0.0123
125	130	60	12.9	0.09	0.0101	0.0224

Table III. - Comparison of results in different operating points

$\boldsymbol{\omega}^*$	Tuning	γ_1^0	γ_2^0	γ_3^0
500	T1	3.92	0.177	0.0281
500	T2	3.98	0.168	0.0283
375	T1	5.25	0.152	0.0290
375	T2	5.34	0.141	0.0295
250	T1	7.37	0.131	0.0289
250	T2	7.34	0.119	0.0293
125	T1	13.77	0.128	0.0277
125	T2	13.83	0.109	0.0284

4. Conclusion

Assessment of controllers is presented in many works by means of a few cases. The results of this paper show that such a procedure is insufficient because two important issues are kept in the dark. First, the trade-offs between figures of merit and second, the relationship between optimal tuning and operating regimes. Without a complete Pareto analysis covering all operating regimes, the conclusions are necessarily baseless.

Acknowledgement

This work is part of the Grant TED2021-129558B-C22 funded by MCIN/AEI/10.13039/501100011033 and by the "European Union NextGenerationEU/PRTR". Also, the authors want to thank the support provided by project I+D+i/PID2021-125189OB-I00, funded by MCIN/AEI/10.13039/501100011033/ by "ERDF A way of making Europe".

References

[1] M. Berenguel, M.R. Arahal, E.F. Camacho, "Modelling the free response of a solar plant for predictive control", Control Engineering Practice (1998), Vol. 6, Iss. 10, pp. 1257–1266.

[2] A. Ramírez-Arias, F. Rodríguez, J.L. Guzmán, M.R. Arahal, M. Berenguel, J.C. López, "Improving efficiency of greenhouse heating systems using model predictive control", IFAC Proceedings Volumes (2005), Vol. 38, Iss. 1, pp. 40–45.

[3] C.S. Lim, E. Levi, M. Jones, N.A. Rahim, W.P. Hew, "FCS-MPC-based current control of a five-phase induction motor and its comparison with PI-PWM control", IEEE Transactions on Industrial Electronics (2013), Vol. 61, Iss. 1, pp. 149–163.

[4] M. Bermúdez, C. Martín, I. González-Prieto, M.J. Durán, M.R. Arahal, F. Barrero, "Predictive current control in electrical drives: an illustrated review with case examples using a five-phase induction motor drive with distributed windings", IET Electric Power Applications (2020), Vol. 14, Iss. 8, pp. 1291–1310.

[5] P.A. de Wit, R. Ortega, I. Mareels, "Indirect field-oriented control of induction motors is robustly globally stable", Automatica (1996), Vol. 32, Iss. 10, pp. 1393–1402.

[6] G. Espinosa-Perez, R. Ortega, "Tuning of PI gains for FOC of induction motors with guaranteed stability", Proceedings of the 23rd International IEEE Conference on Industrial Electronics, Control, and Instrumentation (Cat. No. 97CH36066), IECON 1997, Vol. 2, pp. 569–574.

[7] A.S. Bazanella, R. Reginatto, "Robust tuning of the speed loop in indirect field oriented control of induction motors", Automatica (2001), Vol. 37, Iss. 11, pp. 1811–1818.

[8] M.R. Arahal, M. Duran, "PI tuning of five phase drives with third harmonic injection", Control Engineering Practice (2009), Vol. 17, Iss. 7, pp. 787–797.

[9] R. Ortega, C. Canudas, S.I. Seleme, "Nonlinear control of induction motors: Torque tracking with unknown load disturbance", IEEE Transactions on Automatic Control (1993), Vol. 38, Iss. 11, pp. 1675–1680.

[10] R. Marino, S. Peresada, P. Valigi, "Adaptive input-output linearizing control of induction motors", IEEE Transactions on Automatic control (1993), Vol. 38, Iss. 2, pp. 208–221.

[11] G. Ding, X. Wang, Z. Han, "H$^\infty$ disturbance attenuation control of induction motor", International Journal of Adaptive Control and Signal Processing (2000), Vol. 14, Iss. 2-3, pp. 223–244.

[12] T. Alamo, J.E. Normey-Rico, M.R. Arahal, D. Limon, E.F. Camacho, “Introducing linear matrix inequalities in a control course”, IFAC Proceedings Volumes (2006), Vol. 39, Iss. 6, pp. 205–210.

[13] M. Masiala, B. Vafakhah, J. Salmon, A.M. Knight, “Fuzzy self-tuning speed control of an indirect field-oriented control induction motor drive”, IEEE Transactions on Industry Applications (2008), Vol. 44, Iss. 6, pp. 1732–1740.

[14] N.T. Pham, T.D. Le, “Novel FOC vector control structure using RBF tuning PI and SM for SPIM drives”, International Journal of Intelligent Engineering & Systems (2020), Vol. 13, Iss. 5, pp. 429–440.

[15] L.A. Fernandez-Serantes, J.L. Casteleiro-Roca, J.L. Calvo-Rolle, “Hybrid intelligent system for a half-bridge converter control and soft switching ensurement”, Revista Iberoamericana de Automática e Informática industrial (2022), Vol. 19, Iss. 4, pp. 356–368.

[16] P. Shaija, A.E. Daniel, “Optimal tuning of PI controllers for IM drive using GWO and TLBO algorithms”, 5th International Conference on Electrical, Computer and Communication Technologies, ICECCT 2023, pp. 1–9.

[17] F. Rodríguez, D. Garrido, R. Núñez, G.G. Oggier, G. García, “Feedback linearization control of a dual active bridge converter feeding a constant power load”, Revista Iberoamericana de Automática e Informática Industrial (2023), pp. 237–246.

[18] P. Gonçalves, S. Cruz, A. Mendes, “Finite control set model predictive control of six-phase asymmetrical machines-an overview”, Energies (2019), Vol. 12, Iss. 24, pp. 1–42.

[19] C. Martín, M.R. Arahal, F. Barrero, M.J. Durán, “Multiphase rotor current observers for current predictive control: A five-phase case study”, Control Engineering Practice (2016), Vol. 49, pp. 101–111.

[20] M.G. Satué, M.R. Arahal, D.R. Ramírez, F. Barrero, “Multi-phase predictive control using two virtual voltage-vector constellations”, Revista Iberoamericana de Automática e Informática Industrial (2023), Vol. 20, Iss. 4, pp. 347-354.

[21] H. Zhang, Y. Zhang, Y. Zhu, X. Wang, “Robust deadbeat predictive current control of induction motor drives with improved steady state performance”, IET Power Electronics (2023), Vol. 16, Iss. 8, pp. 1271–1454.

[22] A.G. Yepes, O. Lopez, I. Gonzalez-Prieto, M.J. Duran, J. Doval-Gandoy, “A comprehensive survey on fault tolerance in multiphase AC drives, part 1: General overview considering multiple fault types”, Machines (2022), Vol. 10, Iss. 3, pp. 1–134.

[23] M. Bermúdez, M.R. Arahal, M.J. Duran, I. Gonzalez-Prieto, “Model predictive control of six-phase electric drives including ARX disturbance estimator”, IEEE Transactions on Industrial Electronics (2020), Vol. 68, Iss. 1, pp. 81–91.

[24] A. Cecilia, R. Costa-Castelló, “High gain observer with dynamic deadzone to estimate liquid water saturation in PEM fuel cells”, Revista Iberoamericana de Automática e Informática industrial (2020), Vol. 17, Iss. 2, pp. 169–180.

[25] F. Colodro, J.L. Mora, F. Barrero, M.R. Arahal, J. Martinez-Heredia, “Analysis and simulation of a novel speed estimation method based on oversampling and noise shaping techniques”, Results in Engineering (2024), Vol.21, pp. 1–9.

[26] D. Soto-Marchena, F. Barrero, F. Colodro, M.R. Arahal, J.L. Mora, “On-site calibration of an electric drive: A case study using a multiphase system”, Sensors (2023), Vol. 23, Iss. 17, pp. 1–15.

[27] M.G. Tzitzéica, “Sur une nouvelle classe de surfaces”, Rendiconti del Circolo Matematico di Palermo (1908), Vol. 25, Iss. 1, pp. 180–187.

[28] M.R. Arahal, G. Kowal, F. Barrero, M.M. Castilla, “Cost function optimization for multi-phase induction machines predictive control”, Revista Iberoamericana de Automática e Informática Industrial (2019). Vol. 16, Iss. 1, pp. 48–55.